






Article

The Impact of 3D Printing Process Parameters on the Dielectric Properties of High Permittivity Composites

Athanasios Goulas ^{1,*}, Shiyu Zhang ¹, Darren A. Cadman ¹, Jan Järveläinen ²,
Ville Mylläri ², Will G. Whittow ¹, John (Yiannis) C. Vardaxoglou ¹ and Daniel S. Engström ¹

¹ Wolfson School of Mechanical, Electrical & Manufacturing Engineering, Loughborough University, Loughborough, Leicestershire LE11 3TU, UK; s.zhang@lboro.ac.uk (S.Z.); d.a.cadman@lboro.ac.uk (D.A.C.); w.g.whittow@lboro.ac.uk (W.G.W.); j.c.vardaxoglou@lboro.ac.uk (J.(Y.)C.V.); d.engstrom@lboro.ac.uk (D.S.E.)

² Premix Oy, P.O. Box 12, FI-05201 Rajamäki, Finland; jan.jarvelainen@premixgroup.com (J.J.); ville.myllari@premixgroup.com (V.M.)

* Correspondence: a.goulas@lboro.ac.uk

Received: 30 September 2019; Accepted: 4 November 2019; Published: 5 November 2019



Abstract: Fused filament fabrication (FFF) is a well-known and greatly accessible additive manufacturing technology, that has found great use in the prototyping and manufacture of radiofrequency componentry, by using a range of composite thermoplastic materials that possess superior properties, when compared to standard materials for 3D printing. However, due to their nature and synthesis, they are often a great challenge to print successfully which in turn affects their microwave properties. Hence, determining the optimum printing strategy and settings is important to advance this area. The manufacturing study presented in this paper shows the impact of the main process parameters: printing speed, hatch spacing, layer height and material infill, during 3D printing on the relative permittivity (ϵ_r), and loss tangent ($\tan\delta$) of the resultant additively manufactured test samples. A combination of process parameters arising from this study, allowed successful 3D printing of test samples, that marked a relative permittivity of 9.06 ± 0.09 and dielectric loss of 0.032 ± 0.003 .

Keywords: 3D printing; artificial dielectrics; materials

1. Introduction

For more than two decades, polymers and their functional composites have received great attention due to their potential to be used in a variety of applications in electronics, such as piezo-resistive/electric devices, conductors, etc. [1]. Polymers are typically materials of low relative permittivity or dielectric constant (ϵ_r , where in order to increase their dielectric performance they are infilled with a high dielectric constant ceramic material (e.g., BaTiO₃), in either a micro or nanoparticulate size, to form a polymer composite [2].

Such high dielectric performance polymer composites are of great use in the fabrication of electronic components and lately, they have attracted real interest, for their potential to be integrated into modern radio-frequency (RF) devices operating at microwave frequencies [3]. Ceramic materials have mostly been used in such applications due to their high dielectric constant and low dielectric loss [4], and an enormous amount of research and effort has been afforded for development of novel ceramic materials [5]. However, production of ceramic components comes with several disadvantages such as high tooling costs and challenging implementation, since high temperature processing is required in order to achieve structural integrity and their desired dielectric properties.

Additive manufacturing (AM), commonly known as 3D printing, offers a great deal of flexibility in the manufacture of complex three-dimensional geometries in near net-shape, eliminating any costs associated with tooling and post-processing. Fused filament fabrication (FFF), belongs to the material

extrusion process category, as defined in the ISO/DIS 17296 standard, in which a thermoplastic material is drawn via a heated nozzle and deposits material in layer-by-layer manner to form three-dimensional objects. FFF is a particularly attractive 3D printing process, as it uses equipment of low complexity and it is relatively inexpensive. Despite it being only 30 years old, FFF has only recently become very popular in academia, especially during the past decade. One of the significant events was the expiration of the FFF printing process patent in 2009, which led to a heavy decline in printer prices and made them accessible to the larger public. The commercialization of printers has also boosted the development and commercialization of FFF filaments.

Previously high dielectric constant filaments have been made by stirring dissolved plastics with ceramic particles. This is a time-consuming and expensive method and is nowadays commercially replaced by melt compounding of the components. FFF filaments are typically made in two steps. First, a twin-screw extruder is used to compound the polymer, ceramic filler and various additives to make plastic granules. Secondly, these granules are fed to a machine that makes the 3D-filaments. This machine typically contains a single-screw extruder, precision nozzle, cooling line, haul-off machine and a winder. Additionally, the line can also contain optical scanners to monitor the filament thickness or material driers before the hopper, to achieve good dimensional accuracy.

Although 3D printing in general can be used to manufacture virtually anything, the rise of high permittivity filaments has been mainly due to miniaturization of RF parts in the microwave region. One of the most typical applications where high permittivity filaments have been used is beamforming with flat Fresnel zone or graded index lenses. A desirable lens form factor, i.e., a flat shape, can be achieved using the high permittivity material and varying the infill percentage to obtain an effective ϵ_r , which varies radially along with the lens [6]. Benefits of high permittivity materials have also been demonstrated in antennas [7,8], reflect arrays [9] and dielectric rod waveguides [10].

Very limited work has been reported to date, with regards to high permittivity polymer composite materials suitable for FFF-type 3D printing. Castles et al. reported on the fabrication of a series of composites composed of a BaTiO₃/ABS polymer composite, which could be used with a commercial desktop FFF-type 3D printer to produce parts containing user defined regions of relative permittivity. The authors reported polymer composite blends with ceramic solid loadings of up to 70 wt.%, relative permittivity in the range of $\epsilon_r = 2.6$ –8.7 and loss tangents in the range of 0.005–0.027 [11]. Later on, Wu et al. presented an optimised blend, comprising of BaTiO₃/ABS with volume ration of the infilling material up to 32 vol.% and a maximum relative permittivity value of $\epsilon_r = 11$, in the GHz frequency range [12]. To the best of our knowledge, the studies reported above, cover all the research activities taking place in producing high relative permittivity polymer composites for fused filament fabrication type 3D printing.

However, it would seem that none of these studies have disseminated information with regards to their printability or have investigated how processing conditions are likely to affect the performance of the bulk printed materials. Since FFF has traditionally been used for prototyping purposes, and given its low level and low-cost nature, little attention has been given during the development of the technology to study and optimise the full density of the fabricated components. This is nevertheless expected since FFF-made builds are not intended to be fully functional prototypes and process-related defects, such as porosity/air gaps are not considered important. This is not the case though for dielectric materials, since such imperfections can be detrimental to the performance of the fabricated RF component.

In this work, we present a manufacturing study, using a high permittivity polymer composite filament for FFF-type additive manufacturing. The resulting dielectric properties of the 3D printed samples are assessed, according to the process-related parameters used, such as printing speed, hatch spacing, layer height and material infill.

2. Materials and Methods

The experimental material used in this study was produced by Premix Oy (TP20907, Rajamäki, Finland) in filament form of 1.75 ± 0.1 mm diameter. It is a proprietary composite comprising of an acrylonitrile-butadiene-styrene (ABS) matrix, that contains a ceramic infill of a high relative permittivity.

All manufacturing experiments were carried out on a multi-process additive manufacturing kit (Hydra 16A, Hyrel3D, Norcross, GA, USA) equipped with a filament extrusion module (MK1-250, Hyrel3D, Norcross, GA, USA), fitted with a brass nozzle of 0.5 mm diameter. To assure better adhesion of the first layer, all test samples were printed on adhesive Kapton film of 75 μm thickness, that was placed on top of build surface, heated at 110 °C.

The composite thermoplastic filament was subjected to differential scanning calorimetry (DSC) (2920 Modulated DSC, TA Instruments Inc., New Castle, DE, USA), to identify the thermophysical properties of the material, such as glass transition, decomposition temperature and any other thermophysical material interactions during heating. Those properties helped to identify processing conditions such as the temperature of the build surface and extrusion. DSC was operated under an argon gas environment with a 200 mL/min⁻¹ purging rate, at a heating rate of 10 °C·min⁻¹ from room temperature up to 350 °C. All samples were introduced in high purity aluminium pans with an empty pan used as a reference to calibrate the baseline.

The morphological features of the 3D printed structures, such as internal porosity were investigated using light optical microscopy (LOM) (Eclipse MA200, Nikon Instruments Europe, Netherlands), where the dispersion of the ceramic infilling material into the thermoplastic host was depicted using scanning electron microscopy (SEM) (TM3030 SEM, Hitachi High-Technologies Europe GmbH, Germany). SEM samples were coated with a gold/palladium alloy in an 80:20 weight ratio, for 90 s at 25 mA using a sputter coater (Quorum Q150T, Quorum, Edwards, Hastings, UK).

The dielectric properties of the additively manufactured samples were determined by placing the printed samples of $22.86 \times 10.16 \times 2.5$ mm size, into an X-band waveguide cavity (8.2–12.4 GHz), measuring the transmission and reflection from the target sample, connected to a Vector Network Analyser (VNA) (MS465B22, Anritsu, Japan) using coaxial cables. Relative permittivity (ϵ_r) and loss tangent ($\tan\delta$) were calculated using the Nicolson-Ross-Weir method [13]. All reported measurements are reported as an average out of 5 different 3D printed samples together with standard error.

3. Results and Discussion

Depending on the percentage amount of the infilling material, composites typically exhibit properties such as glass transition or decomposition that are very different to the properties of the host material. According to the manufacturer, this experimental material in these studies that came in the form of a filament suitable for FFF, is a proprietary blend based on an ABS host and contained a high dielectric constant ceramic infill in nanoparticulate form, as shown in Figure 1.

The material was initially subjected to thermal analysis using Differential Scanning Calorimetry (DSC) to identify its thermal behaviour and extract information critical for the successful manufacture of three-dimensional test samples. Calorimetric data revealed a glass transition (T_g) reaction at 105 °C and a major endothermic peak at 290 °C, suggesting complete melting (T_m), as seen in Figure 2.

For thermoplastics, the glass transition (T_g) is the temperature range where the material undergoes a viscous relaxation and behaves as it is in a glassy state; it is strong and rigid but also soft and pliable when it is below the glass transition [14]. In 3D printing of thermoplastics, a temperature slightly above the material's T_g is typically used for heating the built platform. This enables the material to adhere better to the surface, as it leads to a reduction of the surface tension between the printing surface and the printed material, and to a larger contact area that ultimately will cause better adhesion between the bed and the extrudate [15]. Additionally, the build platform's temperature will not allow the extrudate to cool down below its glass transition thereby allowing it to mechanically interlock to the surface characteristics of the build surface, such as porosity and roughness, ensuring proper adherence. A value of 110 °C, corresponding to a temperature slightly above the material's $T_g = 105$

°C, was chosen as the temperature setting for the equipment’s build surface and was similar to most ABS thermoplastic blends typically used for 3D printing.

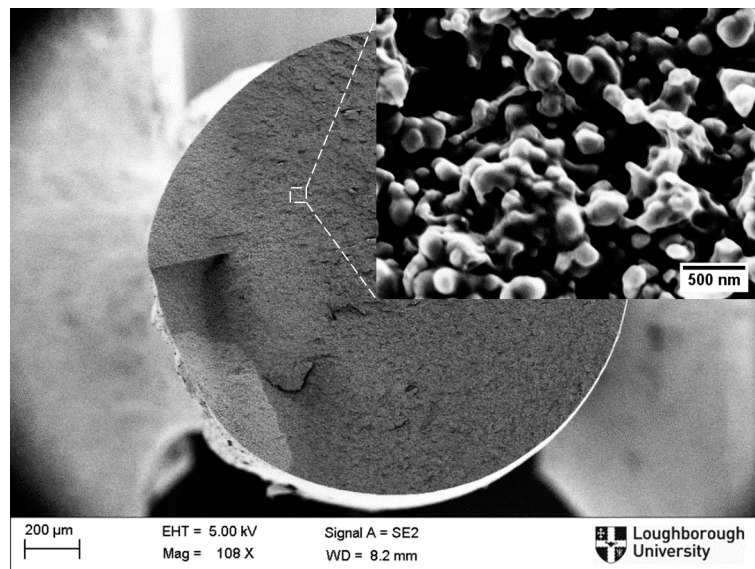


Figure 1. Scanning electron micrograph of the ceramic infill nanoparticles within an ABS matrix.

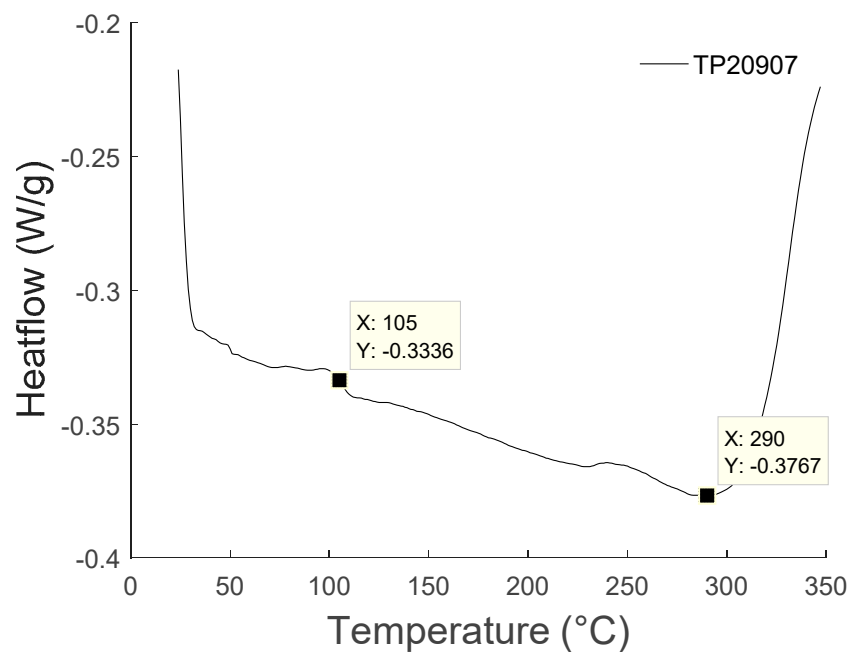


Figure 2. DSC curve of Premix PREPERM™ TP20907.

Most amorphous thermoplastic materials such as ABS do not have a sharply defined melting temperature; they exist in a melt state past their glass transition, but their viscosity is too high to allow for any flow, or any extrusion, as in the case of FFF-type 3D printing. As the material becomes heated, the viscosity reduces significantly, up to a point where the viscosity is low enough to facilitate flow.

DSC data showed a continuous decomposition up to a temperature of 290 °C corresponding to the maximum of the endothermic peak. This suggested that extrusion temperature should not exceed 290 °C to avoid unwanted process repercussions, such as uncontrolled melting and degradation of the thermoplastic polymer. A series of trials, extruding with temperatures below that of 290 °C, determined that 260 °C was the best suited temperature, allowing smooth, continuous and in the overall

defect-free extrusion of the composite material. It should be noted that the extrusion temperature used was unusually high, since ABS-based materials are typically 3D printed using process temperatures between 230–240 °C. This suggested that the amount of the infilling ceramic material had a significant impact on the material's thermal properties and thus on its processability. The higher the solid loading, the higher the viscosity of the composite, therefore higher extrusion temperatures were needed to allow melt flow.

The first process parameter to be investigated was the printing speed with a range of 10–50 mm/s extrusion speeds attempted. The 10–20 mm/s speed range performed well and allowed the successful three-dimensional manufacturing of test samples without any visible defects. However, no successful builds could be achieved when a printing speed passed the 20 mm/s. Test samples printed with speeds in the range of 30–50 mm/s appeared to have several defects during the extrusion process, mainly due to the poor interlaminar bonding between layers, as shown in Figure 3. Additionally, adhesion of the first layer with the build surface appeared to be problematic and was only successful when a printing speed as low as 10 mm/s was used. Therefore, a combination of printing speeds were chosen, 10 mm/s for the bottom layer and 20 mm/s for the rest of the structure, as the most suitable settings for the successful and repeatable manufacture of the test samples in this study.

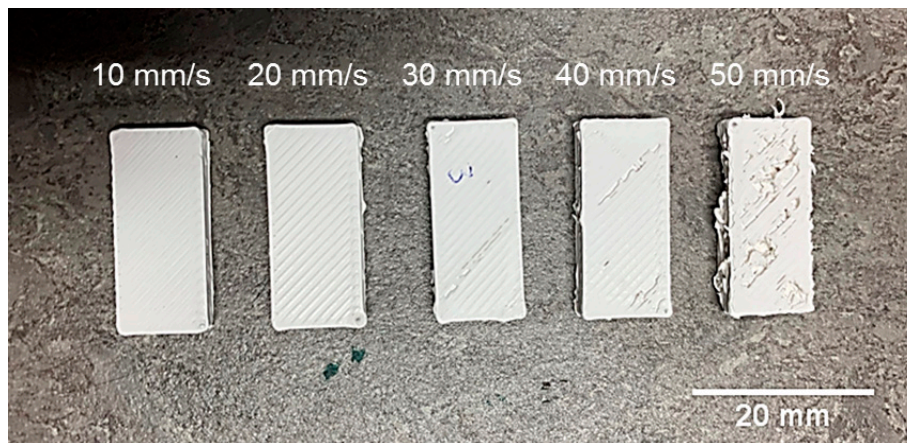


Figure 3. 3D printed test samples using printing speeds of 10–50 mm/s.

Using the above-mentioned printing speeds and a layer thickness of 0.3 mm, a set of 5 rectangular test samples suitable for microwave X-band (8.2–12.4 GHz) waveguide cavities were manufactured and their dielectric properties of interest, such as relative permittivity (ϵ_r) and loss tangent ($\tan\delta$) were calculated using the method stated in the experimental section. It should be noted that no dimensional inaccuracy of the printed samples was observed. There were no obvious airgaps between the 3D printed samples and walls of the waveguide cavity's sample holder.

The additively manufactured test samples, using the above settings, produced a relative permittivity of $\epsilon_r = 7.38 \pm 0.11$ and $\tan\delta = 0.018 \pm 0.005$. The measured relative permittivity was significantly lower than an injection moulded sample that had a relative permittivity of 10 and loss of 0.003 (as measured by the manufacturer at 2.4 GHz using a split-post dielectric resonator). The 3D printed samples were then subjected into a microscopical analysis, using a light optical microscope, as shown in Figure 4, to investigate any likely defects during the printing process which would cause reduced dielectric relative permittivity.

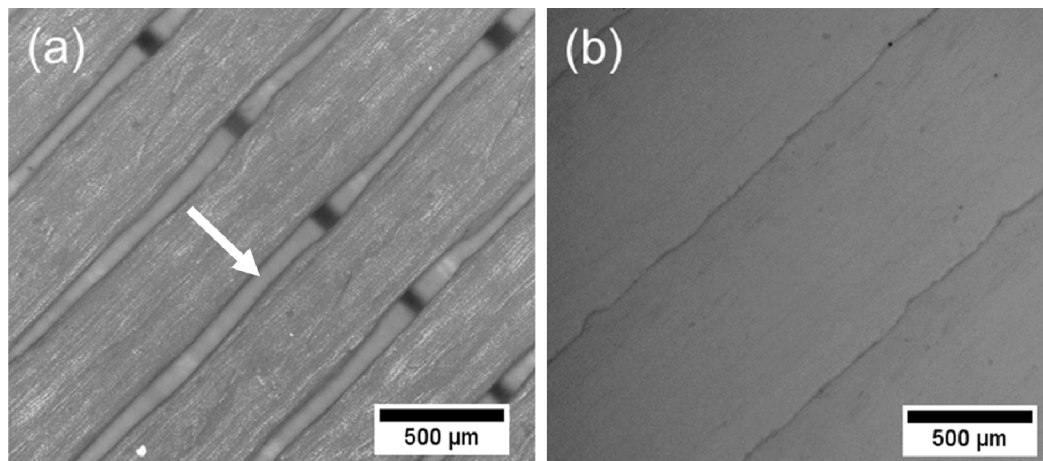


Figure 4. Optical micrograph showing the density of 3D printed samples using (a) 0.5 mm extrusion width versus (b) 0.45 mm extrusion width.

The acquired optical micrographs showed that there was an air gap, in between the individual printed lines forming a single layer. This is shown by the arrow in Figure 4a. This clearly explained the inferior performance in terms of the measured relative permittivity against the bulk material properties, since any voids or air gaps were expected to reduce the measured relative permittivity of the material. The reason for the presence of such air gaps were likely to be caused either: a) due to significant material shrinkage during the cooling down phase of the extrudate, or b) due to non-optimal material flow, which is normally controlled by the software responsible for generating the extrusion parameters during slicing and generation of the g-code. In the first case, this is likely to be the effect of a high solid loading of the ceramic material, affecting the thermophysical properties of the composite. For the latter case, such differences in the extrusion output can be software specific. The algorithm responsible for generating the extrusion parameters in the g-code might differ between the software package used (i.e., Simplify3D, Slic3r, Cura, etc.).

In order to compensate for the above-mentioned shortcoming, the extrusion width that controls the distance between the individual printed lines forming the monolayer was reduced from 0.5 mm to 0.45 mm. This 0.05 mm reduction in the extrusion width matched the dimension of the air gaps, as measured using the previously acquired optical micrographs, as shown in Figure 4. Material flow rate multiplier was left unchanged from its default value of 1, as it would drastically change the amount of material being extruded per given layer thickness and would likely cause over-extrusion, and result in swelling/oozing of the final three-dimensionally printed geometry.

A new set of samples were manufactured, using the adjusted extrusion width value of 0.45 mm and were subsequently measured in the X-band waveguide cavity. Their properties showed a slightly higher relative permittivity and also a lower loss tangent, with values of $\epsilon_r = 7.85 \pm 0.25$, and $\tan\delta = 0.008 \pm 0.011$, as shown in Figure 5. This is clearly explained due to the reduction of any airgaps existing in the continuity of a monolayer. The latter was confirmed by acquiring optical micrographs as shown in Figure 4b. The minor variance in the dielectric performance of the 3D printed samples, as depicted via the error bars, was very likely to be due to inconsistencies during extrusion.

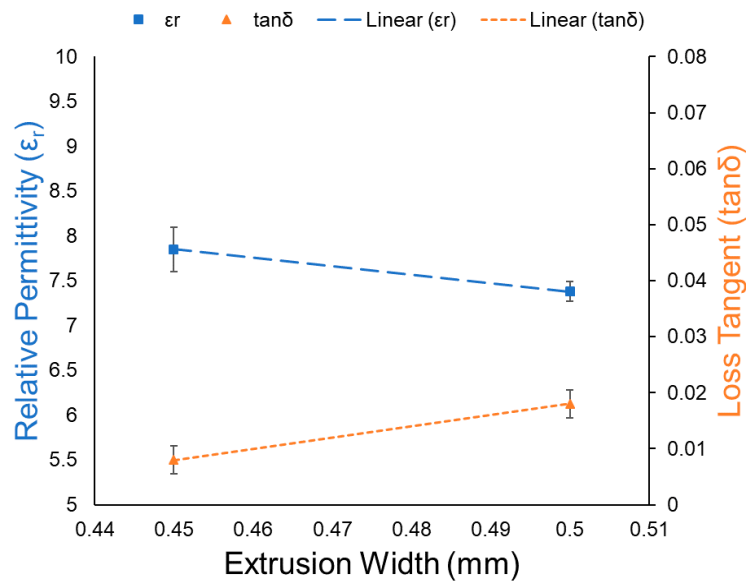


Figure 5. The effect of extrusion width (mm) vs. relative permittivity (ϵ_r) and loss tangent ($\tan\delta$).

A reduced relative permittivity of 3D printed parts is normally associated to process related deficiencies such as unwanted airgaps in between monolayers or even in-between layers. Porosity within FFF additive manufacturing is expected to be at about 15%, even when a fully dense part is set to 3D print, by selecting an infilling factor setting of 100%. As previously stated, this is normally attributed to uncontrolled shrinkage of the thermoplastic material during cooling or even due to material extrusion-related inconsistencies. The latter is significantly more evident with composite materials, as it is rather challenging to achieve a perfectly even dispersion of the infilling material (high dielectric constant ceramic nanoparticles) within the thermoplastic host (ABS), as this would massively affect the glass transition and melting performance of the composite filament.

The next thing to investigate was how the layer height affected the dielectric performance of the built test samples. A series of rectangular test samples were additively manufactured using layer thicknesses ranging from 0.15 to 0.4 mm, following the rule that for better extrusion performance the layer thickness should not exceed 20%–80% of the nozzle’s diameter. The results from built samples, shown in Figure 6, were characterised in the X-band waveguide.

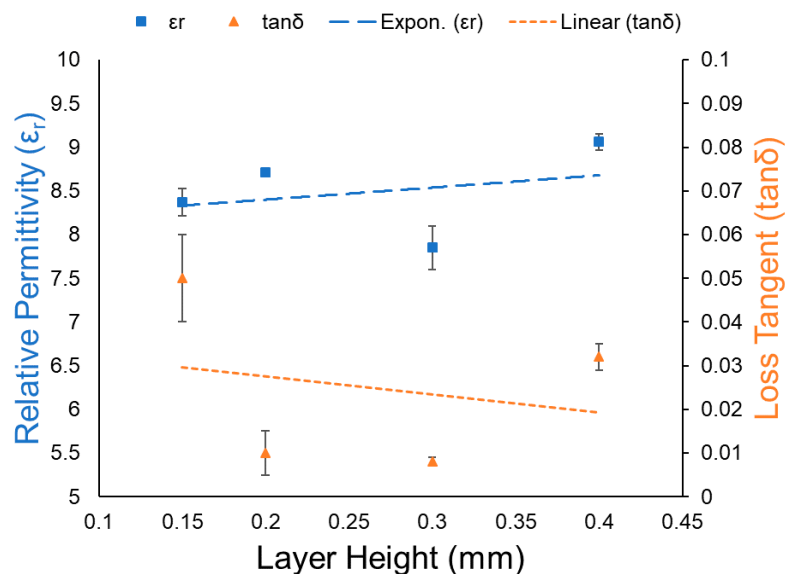


Figure 6. Layer height vs. relative permittivity (ϵ_r) and loss tangent ($\tan\delta$).

As shown in Figure 6, both the relative permittivity and loss tangent values showed a correlation with the varying changing layer height. For a layer height setting of 0.15 mm, dielectric properties of $\epsilon_r = 8.37 \pm 0.16$ and $\tan\delta = 0.05 \pm 0.001$ were measured. However, samples built with a thicker layer height of 0.4 mm demonstrated a higher relative permittivity and lower loss: with dielectric property values as high as $\epsilon_r = 9.06 \pm 0.09$ and $\tan\delta = 0.032 \pm 0.003$. These results are closely comparable to the bulk material’s measured properties, as manufactured via injection moulding, that were $\epsilon_r = 10$ and $\tan\delta = 0.003$. This increased relative permittivity was due to a combination of reasons, such as the reduction of overall porosity within the sample’s volume together with the increased amount of extruded material per given layer height.

It has previously been reported by Zhang et al. that by controlling the amount of the material infill during a print, the relative permittivity could be effectively controlled. This could allow for the manufacture of complex substrates that has locally tailored varied relative permittivity for advanced RF component design [16]. Therefore, a study was carried out to investigate the degree of freedom in controlling the relative permittivity of printed geometries with varied infill factors by using the TP20907 composite ABS, as shown in Figure 7.

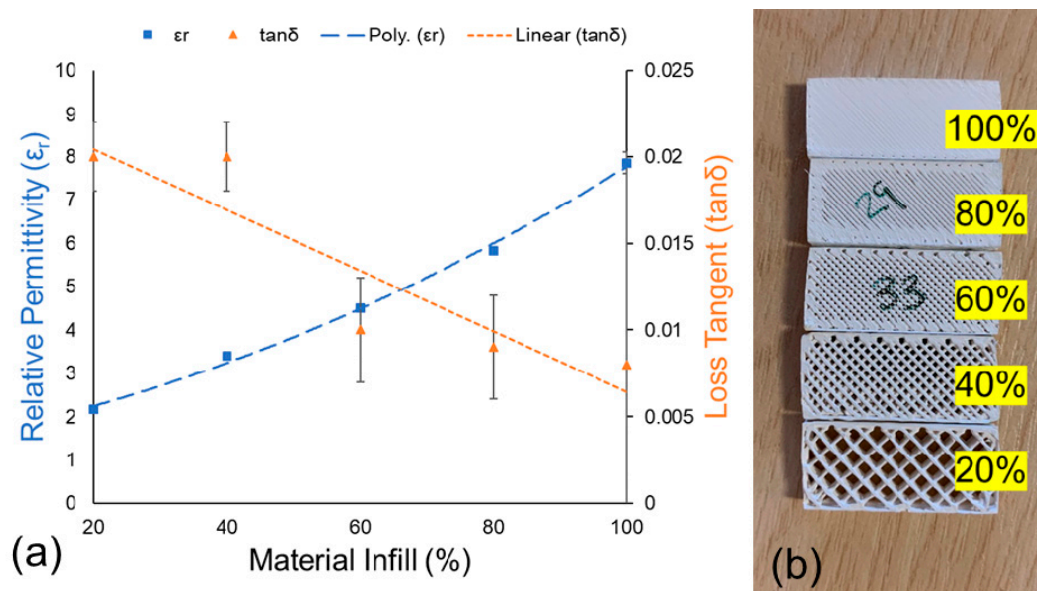


Figure 7. (a) Material Infill (%) vs. relative permittivity (ϵ_r) and loss tangent ($\tan\delta$), (b) Examples of built test samples with variable material infill.

A set of test samples, using infill settings, corresponding to the range of 20%–100% were built. Like the previous process parameters, the infill rate was controlled via the 3D printer’s native software. For clarification, a 20% material infill setting translates to a final geometry of a given volume, that the deposited material accounts for 20% of its overall volume, as shown in Figure 7. The remaining 80% consists of air gaps. It should be noted that interlayer adhesion was very poor when a material infill setting below 20% was chosen and resulted in inferior interlayer adhesion compared with the same partial infilled ABS geometry. This did not allow for the manufacture of any test specimens with infill less than 20%.

Results plotted in Figure 7, demonstrated a clear correlation of the infill factor against the measured relative permittivity (ϵ_r). It was also noted that the reduction in the material infill has a positive effect on the material’s losses. The minimum infill setting of 20% led to a relative permittivity of $\epsilon_r = 2.164 \pm 0.04$ and loss tangent $\tan\delta = 0.02 \pm 0.002$. More advanced RF components, such as planar graded index dielectric lenses [16,17], require a range of dielectric materials with precise specifications which are not commercially available. The above presented approach lends itself to a quick and cost-effective way to produce dielectric materials with bespoke relative permittivity values.

4. Conclusions

FFF is a common and widely adopted 3D printing technology that can also potentially be used for rapid manufacture of functional prototypes for telecommunication and microwave/RF devices. This can be achieved by using composite thermoplastic materials that possess superior dielectric properties, such as: higher relative permittivity (ϵ_r) and low loss ($\tan\delta$), that are hardly realised by conventional thermoplastics. However, the electromagnetic properties of those 3D printed parts are often not comparable to the properties of the bulk material, due to process-related deficiencies subject of the printing parameters being used. The major findings of this paper are summarised in the following bullet points:

- Printing speed was found to have a direct effect on the interlaminar bonding of the 3D printed test samples. It is important to use slower printing speeds with composite thermoplastics, since the ceramic solid infill affects the extrudability of the material. A combination of 10 mm/s for the bottom layer and 20 mm/s for the rest of the structure, gave out successful samples with no macroscopic defects.
- The composite exhibited an approximate volumetric shrinkage of 10% during extrusion. This caused the formation of air voids within the monolayers, leading to the overall reduction of the printed samples' relative permittivity. This was resolved by reducing the hatch spacing parameter and introducing a 10% overlap between the extrudates forming the monolayer.
- The layer height was found to have a significant effect on the 3D printed test samples' dielectric properties. Thicker printed layers performed better, in terms of relative permittivity and loss, when compared to the thinner ones, with values of $\epsilon_r = 9.06 \pm 0.09$, and $\tan\delta = 0.032 \pm 0.003$, corresponding to a 0.4 mm layer height.
- Finally, it was shown that by changing the material infill factor (%), it is possible to effectively control and tailor the properties of the 3D printed structures. Dielectric properties as low as $\epsilon_r = 2.164 \pm 0.04$, and $\tan\delta = 0.02 \pm 0.002$ were recorded, corresponding to a 20% material infill factor. This could enable the fabrication of more advanced RF devices, that rely on graded dielectric properties.

Author Contributions: Conceptualization; investigation; methodology; formal analysis; writing—original draft preparation, A.G.; writing—review and editing, S.Z., D.A.C. and W.G.W.; material development, J.J. and V.M.; supervision, (J.(Y.)C.V.) and D.S.E.; funding acquisition, (J.(Y.)C.V.)

Funding: This work was supported by EPSRC research grant SYMETA (EP/N010493/1).

Acknowledgments: The authors would like to thank the technicians in the Loughborough Materials Characterisation Centre (LMCC) for their help with the analytical equipment.

Conflicts of Interest: The authors declare no conflicts of interest.

References

1. Petrossian, G.; Hohimer, C.J.; Ameli, A. Highly-loaded thermoplastic polyurethane/lead zirconate titanate composite foams with low permittivity fabricated using expandable microspheres. *Polymers* **2019**, *11*, 280. [[CrossRef](#)] [[PubMed](#)]
2. Zhou, T.; Yuan, J.-K.; Li, S.-T.; Hu, G.-H.; Zha, J.-W.; Dang, Z.-M. Fundamentals, processes and applications of high-permittivity polymer–matrix composites. *Prog. Mater. Sci.* **2011**, *57*, 660–723.
3. Chiang, C.K.; Popielarz, R. Polymer Composites with High Dielectric Constant. *Ferroelectrics* **2010**, *275*, 1–9. [[CrossRef](#)]
4. Sebastian, M.T.; Ubic, R.; Jantunen, H. Low-loss dielectric ceramic materials and their properties. *Int. Mater. Rev.* **2015**, *60*, 392–412. [[CrossRef](#)]
5. Muhammad, R.; Iqbal, Y.; Rambo, C.R.; Khan, H. Research trends in microwave dielectrics and factors affecting their properties: A review. *Int. J. Mater. Res.* **2014**, *105*, 431–439. [[CrossRef](#)]
6. Monkevich, J.M.; Le Sage, G.P. Design and Fabrication of a Custom-Dielectric Fresnel Multi-Zone Plate Lens Antenna Using Additive Manufacturing Techniques. *IEEE Access* **2019**, *7*, 61452–61460. [[CrossRef](#)]

7. Espin-Lopez, P.F.; Pasian, M.; Alaimo, G.; Marconi, S.; Auricchio, F.; Heinanen, V.; Jarvelainen, J. 3-D Printed Antenna for Snowpack Monitoring. *IEEE Antennas Wirel. Propag. Lett.* **2018**, *17*, 2109–2113. [[CrossRef](#)]
8. Huang, J.; Chen, S.J.; Xue, Z.; Withayachumnankul, W.; Fumeaux, C. Wideband endfire 3-d-printed dielectric antenna with designable permittivity. *IEEE Antennas Wirel. Propag. Lett.* **2018**, *17*, 2085–2089. [[CrossRef](#)]
9. Zhang, S. Three-dimensional printed millimetre wave dielectric resonator reflectarray. *IET Microw. Antennas Propag.* **2017**, *11*, 2005–2009. [[CrossRef](#)]
10. Lugo, D.C.; Ramirez, R.A.; Castro, J.; Wang, J.; Weller, T.M. 3D printed multilayer mm-wave dielectric rod antenna with enhanced gain. In Proceedings of the 2017 IEEE International Symposium on Antennas and Propagation & USNC/URSI National Radio Science Meeting, San Diego, CA, USA, 9–14 July 2017; pp. 1247–1248.
11. Castles, F.; Isakov, D.; Lui, A.; Lei, Q.; Dancer, C.E.J.; Wang, Y.; Janurudin, J.M.; Speller, S.C.; Grovenor, C.R.M.; Grant, P.S. Microwave dielectric characterisation of 3D-printed BaTiO₃/ABS polymer composites. *Sci. Rep.* **2016**, *6*, 1–8. [[CrossRef](#)] [[PubMed](#)]
12. Wu, Y.; Isakov, D.; Grant, P.S. Fabrication of composite filaments with high dielectric permittivity for fused deposition 3D printing. *Materials* **2017**, *10*, 1218. [[CrossRef](#)] [[PubMed](#)]
13. Lee, C.; McGhee, J.; Tsiopogiannis, C.; Zhang, S.; Cadman, D.; Goulas, A.; Whittaker, T.; Gheisari, R.; Engstrom, D.; Vardaxoglou, J.C.; et al. Evaluation of Microwave Characterization Methods for Additively Manufactured Materials. *Designs* **2019**, *3*, 47. [[CrossRef](#)]
14. Kalogeras, I.M. Glass-Transition Phenomena in Polymer Blends. *Encycl. Polym. Blends* **2016**, *3*, 1–134.
15. Spoerk, M.; Gonzalez-Gutierrez, J.; Sapkota, J.; Schuschnigg, S.; Holzer, C. Effect of the printing bed temperature on the adhesion of parts produced by fused filament fabrication. *Plast. Rubber Compos.* **2018**, *47*, 17–24. [[CrossRef](#)]
16. Zhang, S.; Arya, R.K.; Pandey, S.; Vardaxoglou, Y.; Whittow, W.; Mitra, R. 3D-printed planar graded index lenses. *IET Microw. Antennas Propag.* **2016**, *10*, 1411–1419. [[CrossRef](#)]
17. Zhang, S.; Vardaxoglou, Y.; Whittow, W.; Mitra, R. 3D-printed graded index lens for RF applications. In Proceedings of the 2016 International Symposium on Antennas and Propagation (ISAP), Okinawa, Japan, 24–28 October 2016; pp. 90–91.



© 2019 by the authors. Licensee MDPI, Basel, Switzerland. This article is an open access article distributed under the terms and conditions of the Creative Commons Attribution (CC BY) license (<http://creativecommons.org/licenses/by/4.0/>).